

# Computer Methods in Biomechanics and Biomedical Engineering

ISSN: 1025-5842 (Print) 1476-8259 (Online) Journal homepage: <http://www.tandfonline.com/loi/gcmb20>

## Biomechanical analysis of lumbar interbody fusion cages with various lordotic angles: a finite element study

Zhenjun Zhang, Guy R. Fogel, Zhenhua Liao, Yitao Sun & Weiqiang Liu

To cite this article: Zhenjun Zhang, Guy R. Fogel, Zhenhua Liao, Yitao Sun & Weiqiang Liu (2018): Biomechanical analysis of lumbar interbody fusion cages with various lordotic angles: a finite element study, *Computer Methods in Biomechanics and Biomedical Engineering*, DOI: [10.1080/10255842.2018.1442443](https://doi.org/10.1080/10255842.2018.1442443)

To link to this article: <https://doi.org/10.1080/10255842.2018.1442443>



Published online: 07 Mar 2018.



Submit your article to this journal [↗](#)



View related articles [↗](#)



View Crossmark data [↗](#)



# Biomechanical analysis of lumbar interbody fusion cages with various lordotic angles: a finite element study

Zhenjun Zhang<sup>a,b</sup>, Guy R. Fogel<sup>c</sup>, Zhenhua Liao<sup>b</sup>, Yitao Sun<sup>d</sup> and Weiqiang Liu<sup>a,b</sup>

<sup>a</sup>Department of Mechanical Engineering, Tsinghua University, Beijing, China; <sup>b</sup>Biomechanics and Biotechnology Lab, Research Institute of Tsinghua University in Shenzhen, Shenzhen, China; <sup>c</sup>Spine Pain Begone Clinic, San Antonio, TX, USA; <sup>d</sup>Haicheng City Central Hospital, Haicheng, China

## ABSTRACT

Inappropriate lordotic angle of lumbar fusion cage could be associated with cage damage or subsidence. The biomechanical influence of cage lordotic angle on lumbar spine has not been fully investigated. Four surgical finite element models were constructed by inserting cages with various lordotic angles at L3-L4 disc space. The four motion modes were simulated. The range of motion (ROM) decreased with increased lordotic angle of cage in flexion, extension, and rotation, whereas it was not substantially changed in bending. The maximum stress in cage decreased with increased lordotic angle of cage in all motion modes. The maximum stress in endplate at surgical level increased with increased lordotic angle of cage in flexion and rotation, whereas it was not substantially changed in extension and bending. The facet joint force (FJF) was much smaller than that for the intact conditions in extension, bending, and rotation, while it was not substantially changed in flexion. In conclusion, the ROM, stresses in the cage and endplate at surgical level are sensitive to the lordotic angle of cage. The increased cage lordotic angle may provide better stability and reduce the risk of cage damage, whereas it may increase the risk of subsidence in flexion and rotation.

## ARTICLE HISTORY

Received 27 August 2017  
Accepted 14 February 2018

## KEYWORDS

Lumbar spine; biomechanics; interbody cage; finite element analysis (FEA); subsidence; facet contact force

## 1. Introduction

Lateral lumbar interbody fusion has been widely performed for degenerative lumbar disease, and the implantation of the lordotic cage was thought to contribute to lordosis restoration (Knight et al. 2009; Dakwar et al. 2010; Kim, Lee et al. 2014; Sembrano et al. 2017). A recent clinical and radiological study indicated that the 12° lordotic cage seemed to result in more disc angle and less subsidence (Kim, Lee et al. 2014). According to the recent finite element study, the increased segmental lumbar lordosis could be achievable by using lordotic cages (Uribe et al. 2012, 2015). In addition, it was known that Nuvasive (Nuvasive, Inc., San Diego, CA) went from 10° to 15° lordosis on their standard cages, but we have not found related studies on subsidence effect of 50% increase in degrees of lordosis. A finite element study is necessary to elucidate the influence of the lordotic angle of interbody cages on the subsidence.

It was known that some factors could contribute to subsidence risk, such as cage design and implant position, bone

quality of vertebral trabecular and endplate, and preparation of endplate. However, according to the existing literature, the etiology of subsidence is not fully understood. It was necessary to study the biomechanical effects of interbody cages with various lordotic angles using a lumbar spine model, as well as damage to the adjacent levels induced by the increased stiffness in the surgical level related to the interbody cage. The aim of this study was to investigate the biomechanical properties of interbody cages with various lordotic angles using finite element method (FEM).

## 2. Materials and methods

The FE model of the intact lumbar spine employed in this study was developed and validated in our previous study (Zhang et al. 2017). A total of 492 computed tomography (CT) images of lumbar spine with interval of 0.7 mm were obtained from a healthy woman (age 36 yr, height 158 cm, weight 52 kg), excluded from lumbar disease by visual and radiographic examination. The CT image data was imported into medical image analysis and processing software Mimics (Materialise Inc, Leuven, Belgium).

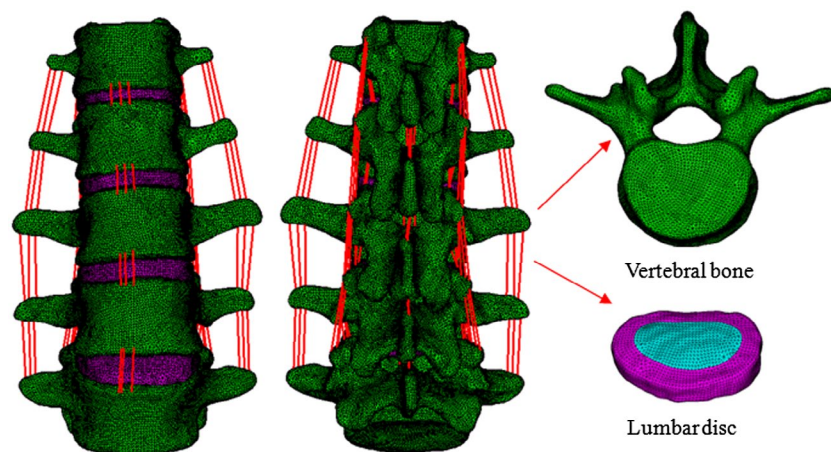
The three-dimensional (3D) geometric model was reconstructed using Mimics. The 3D geometric model consists of vertebrae (L1, L2, L3, L4, and L5), intervertebral discs (D1, D2, D3, and D4) and cartilage endplates. The geometric model was meshed using preprocessing software Hypermesh (Altair Technologies Inc, Fremont, CA). Lastly, the model was imported into FE software Abaqus (Simulia Inc, Providence, RI) to perform FEA. The workstation used for the simulation was ThinkStation (Lenovo, China) configured with 64 GB memory and 24 processors.

Figure 1 displayed the FE model of the intact lumbar spine. Each vertebra was divided into three parts: cancellous bone, cortical bone, and posterior bone. Each intervertebral disc was divided into two parts: annulus fibrosus and nucleus pulposus. 7 kinds of ligaments were included in the FE model: anterior longitudinal ligament (ALL), posterior longitudinal ligament (PLL), ligamenta flava (LF), interspinous ligament (ISL), supraspinous ligament (SSL), intertransverse ligament (ITL), and capsular ligament (CL). The thickness of cortical bone was 1.0 mm, and the thickness of bone endplate was 0.5 mm (Ambati et al. 2015). All kinds of ligaments were modeled as truss elements (T3D2) which had the property of tension-only. The 3D tetrahedral elements were employed to mesh the FE model except for the ligaments. 195,533 nodes and 841,038 elements were contained in the intact FE model, which could effectively eliminate the influence of meshing on the accuracy of the calculation.

The interbody cages with various lordotic angles were modeled based on Nuvasive cage (Nuvasive, Inc., San Diego, CA). The lordotic angle of the reference cage was 15°, the anterior height was 10 mm, and the posterior height was 4 mm. The cage was made of polyetheretherketone (PEEK). The bilateral pedicle screw system was modeled based on EXPEDIUM 5.5 System (DePuy Synthes Spine, Inc, Raynham, MA). The diameter of pedicle screw was 5.5 mm. The pedicle screw was made of titanium alloy

(Ti6Al4 V). The material properties of components were shown in Table 1 (Shirazi-Adl et al. 1986; Chosa et al. 2004; Vadapalli et al. 2006; Zhong et al. 2006; Schmidt et al. 2007; Ayturk and Puttitz 2011; Xiao et al. 2012; Dreischarf et al. 2014; Faizan et al. 2014).

Two steps of simulation were implemented to validate the intact FE model. The predicted results were compared with the previous experimental data. The interfaces of vertebrae and intervertebral discs were assigned to tie constraints. The interfaces of adjacent facet joints were assigned as nonlinear frictionless sliding contact (Shirazi-Adl et al. 1986; Zhong et al. 2006; Schmidt et al. 2007; Ayturk and Puttitz 2011; Dreischarf et al. 2014). First of all, the convergence analysis was performed using the results of intervertebral disc pressure (IDP). The intervertebral disc of the motion segment L4-L5 was meshed with different mesh sizes (0.5, 1.0, and 2.0 mm) to establish three models (Model-0.5, Model-1.0, and Model-2.0). The IDP of the three models under pure compression 400 N was calculated. According to the results of convergence validation, the mesh size was chosen. The compression-displacement of the motion segment L4-L5 under pure compression was calculated. The upper surface of L4 was applied with increasing preload values (100 N, 200 N, 300 N, and 400 N) as described by Berkson et al. (1979). The compression-displacement and IDP of L4-L5 were also compared with the previous experimental results (Berkson et al. 1979; Brinckmann and Grootenboe 1991; Schmidt et al. 2012). Then the range of motion (ROM) of intact lumbar spine L1-L5 under pure moment was predicted. The increasing moments (2.5, 5.0, and 7.5 Nm) were applied to the upper surface of L1 while the bottom of L5 was fixed. The predicted total ROM of L1-L5 was compared with the previous experimental results (Schmidt et al. 2012; Dreischarf et al. 2014). The validation results of intact FE model was reported in our previous study (Zhang et al. 2017).



**Figure 1.** FE model of intact lumbar spine.

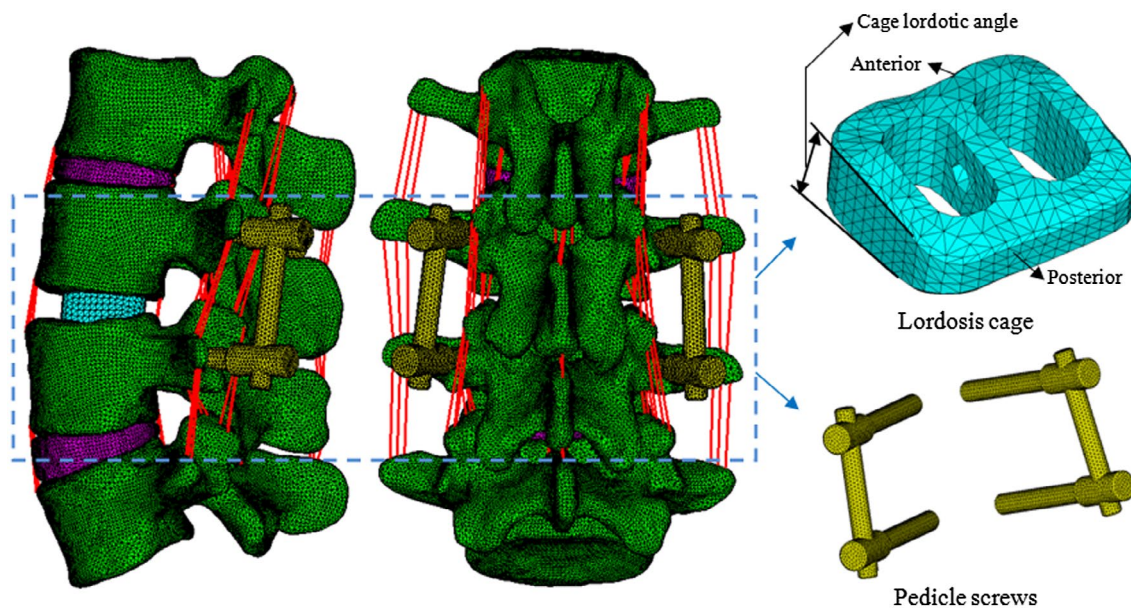
**Table 1.** Material properties of components in the FE models.

Components	Young's modulus (MPa)	Poisson ratio	Cross-sectional area (mm <sup>2</sup> )	References
Cortical bone	12,000	0.3	–	Shirazi-Adl et al. (1986), Zhong et al. (2006)
Cancellous bone	100	0.2	–	Shirazi-Adl et al. (1986), Zhong et al. (2006)
Posterior bone	3500	0.25	–	Shirazi-Adl et al. (1986), Zhong et al. (2006)
Endplate	4000	0.3	–	Schmidt et al. (2007)
Annulus fibrosus	4.2	0.45	–	Shirazi-Adl et al. (1986), Zhong et al. (2006)
Nucleus pulposus	1	0.49	–	Ayturk and Puttlitz (2011), Dreischarf et al. (2014)
ALL	20	0.3	63.7	Zhong et al. (2006), Faizan et al. (2014)
PLL	20	0.3	20	Zhong et al. (2006), Faizan et al. (2014)
LF	19.5	0.3	40	Zhong et al. (2006), Faizan et al. (2014)
ISL	11.6	0.3	40	Zhong et al. (2006), Faizan et al. (2014)
SSL	15	0.3	30	Zhong et al. (2006), Faizan et al. (2014)
TL	58.7	0.3	3.6	Zhong et al. (2006), Faizan et al. (2014)
CL	32.9	0.3	60	Zhong et al. (2006), Faizan et al. (2014)
Cage (PEEK)	3500	0.3	–	Vadapalli et al. (2006), Xiao et al. (2012)
Pedicle screws (Titanium alloy)	110,000	0.3	–	Chosa et al. (2004), Xiao et al. (2012)

Notes: (ALL, anterior longitudinal ligament; PLL, posterior longitudinal ligament; LF, ligamentum flavum; ISL, interspinous ligament; SSL, supraspinous ligament; TL, transverse ligament; CL, capsular ligament.).

To simulate the surgical conditions, the segment L2-L5 was chosen to predict the biomechanical changes after inserting the cages with various lordotic angles. The interbody cage was inserted into the L3-L4 disc space laterally according to the clinical situation. The surgical conditions were ALL intact and supplemental bilateral pedicle screws. The various lordotic angles of cages were 0° (Cage0), 5° (Cage5), 10° (Cage10), and 15° (Cage15). The surgical FE models with various lordotic cages were shown in Figure 2. All the four surgical FE models were constructed based on the validated intact model. The interfaces of the vertebrae and discs, and the surface contact between the facet joints were consistent with that of the intact model. The

interfaces of vertebrae and cages were also assigned to tie constraints. The bottom of L5 was fixed in all directions. The combined load of 280 N and 7.5 Nm were applied on the upper surface of L2 as in previous literature (Rohlmann et al. 2001; Choi et al. 2016; Zhang et al. 2017). The compressive load corresponded to the partial weight of a human body. The moments simulated the different motion modes. Taking into account the symmetrical sagittal plane, the four motion modes (flexion, extension, left bending, and left rotation) was simulated for surgical FE models in this study. The main biomechanical parameters were analyzed and exported, including ROM, cage stress, IDP, endplate stress, and facet joint force (FJF). The ROM

**Figure 2.** Surgical FE model with lordotic cages.



data were normalized to the intact ROM data. Under the combined load of 280 N and 7.5 Nm, the intact L2-L5 model was recalculated. A total of 20 simulation calculations for five models and four motion modes were performed. Simulation results were in accordance with the requirements of visualization, and mechanics data was expressed using Von Mises stress contours. The maximum Von Mises stresses were exported as cage stress, IDP, and endplate stress in this study.

### 3. Results

#### 3.1. Model validation

Under the pure compression, the IDP of the L4-L5 segment was displayed in Figure 3(a) and (b). Compared with Model-0.5, the IDP for Model-1.0 was changed by  $-4.58\%$ , and the IDP for Model-2.0 changed by  $-37.3\%$ . The element size of 1.0 mm was chosen in this study, which is also comparable to the previous study (Xiao et al. 2012). Figure 3(c) showed the compression-displacement curves, which demonstrated that the axial displacement of L4-L5 increased almost linearly with the increased axial compressive loading. Compared with the

previous *in vitro* experimental study (Berkson et al. 1979), the predicted results were reasonable and reliable. Figure 3(d) displayed the compression-IDP curves, which were compared with the previous FE and *in vitro* experimental studies (Brinckmann and Grootenboe 1991; Schmidt et al. 2012). The predicted results indicated that IDP of L4-L5 increased almost linearly with the increased axial compressive loading.

The FE model of the intact lumbar spine has been validated in our previous study (Zhang et al. 2017). When the pure moment of 7.5 Nm was applied, the total ROM was within the range of the previous FE and *in vitro* experimental results (Schmidt et al. 2012; Dreischarf et al. 2014). The load-deflection curves were comparable with the existing results of previous studies (Schmidt et al. 2012; Dreischarf et al. 2014).

#### 3.2. Range of motion (ROM)

Under the combined load of 280 N and 7.5 Nm, the predicted ROM of surgical models was shown in Figure 4. After implantation of interbody cages, the ROM at surgical level L3-L4 decreased substantially in all motion modes. The ROM at surgical level decreased with increased

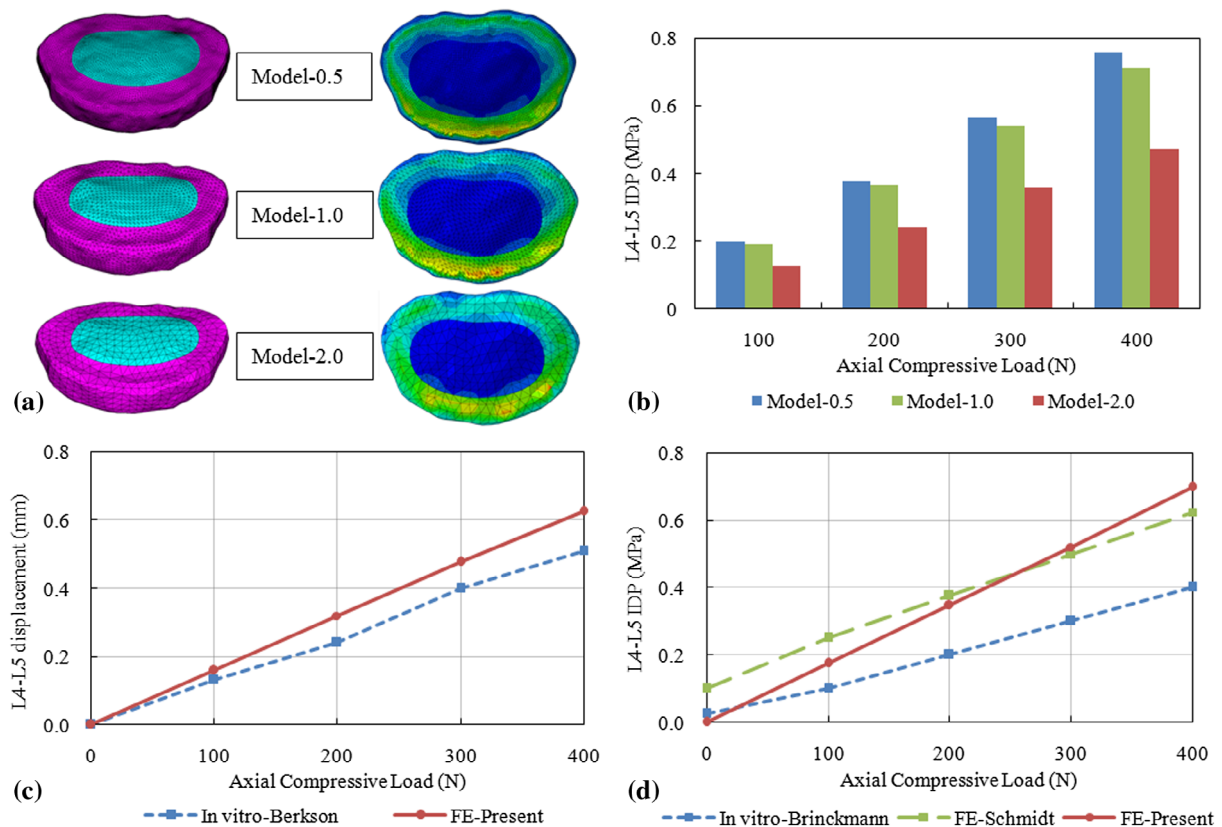


**Figure 3.** Predicted contour plots of Von Mises stress in the intervertebral disc for different models (a) and IDP for different models (b), and compression-displacement curves (c) and compression-IDP curves (d) under axial compression. (IDP, maximum Von Mises stress in the intervertebral disc.).

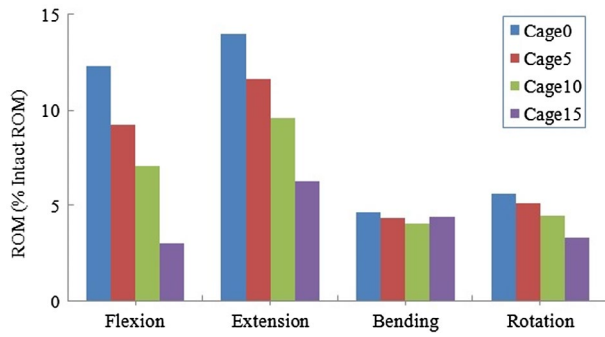


**Figure 4.** ROM at surgical level with various cage lordotic angles in four motion modes. (ROM, range of motion).

lordotic angle of cage in flexion, extension, and rotation, whereas it was changed very little in bending. Compared with Cage0, ROM for Cage5, Cage10, and Cage15 was changed by  $-25.01$ ,  $-42.34$ , and  $-75.64\%$  in flexion,  $-17.01$ ,  $-31.43$ , and  $-55.17\%$  in extension,  $-6.57$ ,  $-12.16$ , and  $-5.31\%$  in bending,  $-9.30$ ,  $-20.29$ , and  $-40.82\%$  in rotation, respectively.

### 3.3. Cage stress and IDP

The maximum stress in cage was shown in Figure 5. The maximum stress in cage decreased with increased lordotic angle in all motion modes. Compared with Cage0, the maximum stresses in cage for Cage5, Cage10, and Cage15 was changed by  $-20.61$ ,  $-50.76$ , and  $-77.81\%$  in flexion,  $-23.95$ ,  $-41.27$ , and  $-61.35\%$  in extension,  $-35.32$ ,  $-43.79$ , and  $-62.00\%$  in bending,  $-4.15$ ,  $-14.30$ , and  $-84.11\%$  in rotation, respectively. The IDP at adjacent levels was shown in Figure 6. Compared among surgical models, the IDP at adjacent levels was not substantially changed with increased lordotic angles of cage. However, the IDP at adjacent level L2-L3 after interbody fusion increased to about twice the intact model in extension.

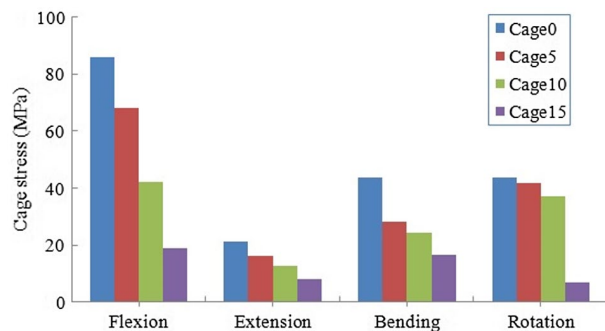


**Figure 5.** Maximum Von Mises stress in the cage with various cage lordotic angles in four motion modes.

### 3.4. Endplate stress

Figure 7 showed the maximum stress in the L3 inferior endplate of surgical models. After implantation of interbody cages, the endplate stress at surgical level L3-L4 increased in all motion modes. The endplate stress at surgical level L3-L4 increased with increased lordotic angle of cage in flexion and rotation, whereas it was not substantially changed in extension and bending. Compared with Cage0, the maximum stress in endplate for Cage5, Cage10, and Cage15 was changed by  $26.10$ ,  $45.49$ , and  $103.69\%$  in flexion,  $-0.83$ ,  $0.58$ , and  $15.04\%$  in extension,  $-9.68$ ,  $-14.56$ , and  $-3.62\%$  in bending,  $0.98$ ,  $12.15$ , and  $40.25\%$  in rotation, respectively.

### 3.5. Facet joint force (FJF)

Figure 8 displayed the FJF of the surgical models. After implantation of interbody cages, the FJF at surgical level L3-L4 decreased substantially in all motion modes except for flexion. Compared among surgical models, the FJF at surgical level L3-L4 was not changed substantially with increased lordotic angle in flexion and extension. In bending and rotation, the FJF at surgical level was sensitive to the cage lordotic angle. Compared with Cage0, the FJF for Cage5, Cage10, and Cage15 was changed by  $-7.51$ ,  $-9.06$ , and  $-10.92\%$  in flexion,  $-2.48$ ,  $-4.14$ , and  $-6.02\%$  in extension,  $5.12$ ,  $11.15$ , and  $25.78\%$  in bending,  $-3.99$ ,  $-8.48$ , and  $-18.18\%$  in rotation, respectively.

## 4. Discussion

The predicted ROM with various cage lordotic angles was comparable to the previous studies (Beaubien et al. 2005; Slucky et al. 2006; Cappuccino et al. 2010). In addition, the current study showed the cage stress, IDP, endplate stress, and FJF. As was displayed in Figure 4, the ROM at surgical level L3-L4 decreased substantially after inserting the lordotic cages in all the motion modes. As was displayed in Figures 5 and 6, the maximum stress in cage decreased substantially with increased lordotic angle, whereas the maximum stress in endplate increased with increased lordotic angle in flexion and rotation. The cage stress and endplate stress at surgical level L3-L4 were sensitive to the cage lordotic angle. Compared among the cages with various lordotic angles, the  $15^\circ$  lordotic cage displayed some advantages at surgical level, such as the minimum ROM in flexion, extension and rotation, the minimum cage stress in all motion modes, and the minimum FJF in flexion, extension and rotation. However, the endplate stress for  $15^\circ$  lordotic cage was the maximum in flexion, extension, and rotation. The results indicated that the increased cage lordotic angle may improve lumbar stability and reduce

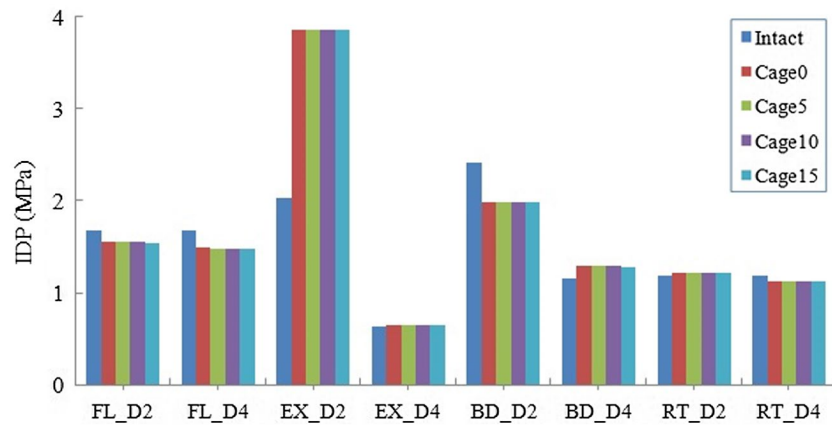


**Figure 6.** IDP at adjacent levels with various cage lordotic angles in four motion modes. (IDP, maximum Von Mises stress in the intervertebral disc; FL, flexion; EX, extension; BD, bending; RT, rotation; D2, disc between L2 and L3; D4, disc between L4 and L5.).

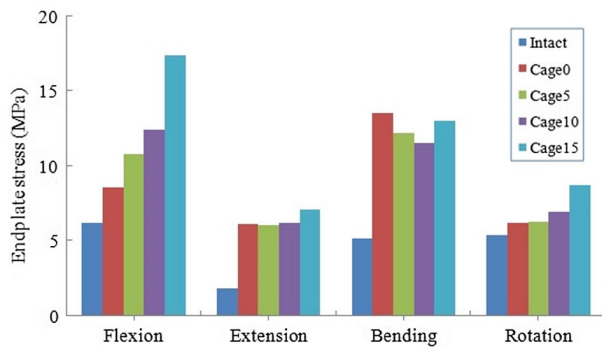


**Figure 7.** Maximum Von Mises stress in the L3 bottom endplate with various cage lordotic angles in four motion modes.

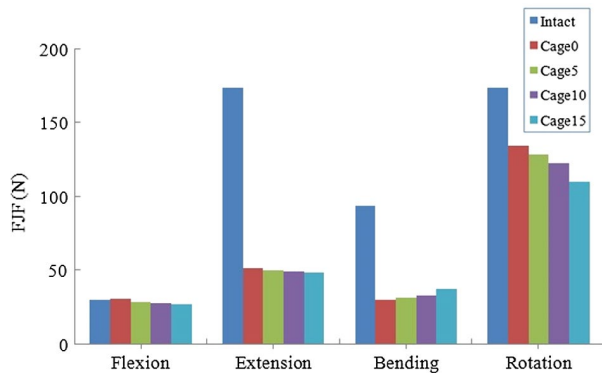


**Figure 8.** FJF at surgical level with various cage lordotic angles in four motion modes. (FJF, facet joint force).

the risk of cage damage, while it may increase the risk of subsidence in flexion and rotation.

The basic idea of lumbar fusion is to stabilize the lumbar spine by reducing the ROM at surgical level. Some literatures have shown that lumbar fusion may cause a stress shielding effect, which may accelerate the intervertebral disc degeneration at adjacent levels (Kim, Kang et al. 2014; Zhang et al. 2016). In Figure 6, the IDP at L2-L3

increased substantially after fusion in extension, while it showed similar results with the case of intact model in other motion modes. Because the same load condition was considered in the present study, the IDP at adjacent levels was not substantially changed in all motion modes except for extension. However, in order to achieve the desired total ROM, patients after interbody fusion will increase the driving force naturally, which may further increase the risk of intervertebral disc degeneration at adjacent levels.

In this study, Nuvasive 15° lordotic cage was chosen as reference cage according to the foraminal height and disc angle of the present lumbar model. In the previous studies on lumbar fusion it was shown that bilateral pedicle screw fixation provides superior biomechanical stability in lateral lumbar interbody fusion (Kim, Kang et al. 2014; Ambati et al. 2015). In the present study, the surgical conditions were chosen according to the clinical practice (Figure 2). This FE study may explain the relationship between cage lordotic angle and risk of subsidence. However, optimal design of the geometry of interbody cage and the methods of reducing subsidence still need further investigation. The next work for our team is to optimize the anterior geometry of an interbody cage which may reduce the endplate stress in flexion, and to implant a lateral plate which might help a little in bending and rotation.

There are some limitations in this finite element study, such as using a unique lumbar model, simplifying the material properties of some tissues, and ignoring the role of muscles. First of all, the geometric model of lumbar spine varies from person to person, such as disc height and the joint space. But in the present study only one model of lumbar spine was chosen. Secondly, although the components of lumbar spine are nonlinear in reality, the material properties of them were simplified as linear elastic in this study. However, many FEA on lumbar spine have assumed that the components was linear in order to improve the calculation efficiency (Grauer et al.

2006; Vadapalli et al. 2006; Zhong et al. 2006; Kim et al. 2010; Choi et al. 2016; Zhang et al. 2017). In addition, the muscles have an important contribution to support the stability of lumbar spine. But the muscles were not considered in this study. However, the tendency of predicted results with varied lordotic angles of cage would not be substantially changed depending on the personalized geometric model, material properties of components, and model of the muscles.

## 5. Conclusion

According to the predicted results of the FEA, it was shown that the lordotic angle of interbody cage can affect the biomechanics of lumbar spine noticeably. Compared among the cages with different lordotic angles, the 15° lordotic cage showed some advantages in reducing the ROM, cage stress and FJF. This may explain the reason why Nuvasive went from 10° to 15° lordosis on their standard cages from a biomechanical point of view. However, the increased cage lordotic angle may increase the risk of subsidence. The predicted results indicated further investigation seems to be necessary to reduce the endplate stress, such as optimal design of the anterior geometry of cages and comparing various supplemented fixation options.

## Disclosure statement

No potential conflict of interest was reported by the authors.

## Funding

This work was supported by the Industry Public Technology Service Platform Project of Shenzhen [grant number SMJKPT20140417010001], and the Science and Technology Plan Basic Research Project of Shenzhen [grant number JCYJ20151030160526024].

## References

- Ambati DV, Wright EK, Lehman RA, Kang DG, Wagner SC, Dmitriev AE. 2015. Bilateral pedicle screw fixation provides superior biomechanical stability in transforaminal lumbar interbody fusion: a finite element study. *Spine J.* 15:1812–1822.
- Ayturk UM, Puttlitz CM. 2011. Parametric convergence sensitivity and validation of a finite element model of the human lumbar spine. *Comput Methods Biomech Biomed Eng.* 14:695–705.
- Beaubien BP, Derincek A, Lew WD, Wood KB. 2005. In vitro, biomechanical comparison of an anterior lumbar interbody fusion with an anteriorly placed, lowprofile lumbar plate and posteriorly placed pedicle screws or translamina screws. *Spine.* 30:1846–1851.
- Berkson MH, Nachemson A, Schultz AB. 1979. Mechanical properties of human lumbar spine motion segments – Part II: responses in compression and shear; influence of gross morphology. *J Biomech Eng.* 101:53–57.
- Brinckmann P, Grootenboe H. 1991. Change of disc height, radial disc bulge, and intradiscal pressure from discectomy an *in vitro* investigation on human lumbar discs. *Spine.* 16:641–646.
- Cappuccino A, Cornwall GB, Turner A, Fogel GR, Duong HT, Kim KD, Brodke DS. 2010. Biomechanical analysis and review of lateral lumbar fusion constructs. *Spine.* 35:S361–S367.
- Choi J, Shin D, Kim S. 2016. Biomechanical effects of the geometry of ball-and-socket artificial disc on lumbar spine: A finite element study. *Spine.* 42:E332–E339.
- Chosa E, Goto K, Totoribe K, Tajima N. 2004. Analysis of the effect of lumbar spine fusion on the superior adjacent intervertebral disk in the presence of disk degeneration, using the three-dimensional finite element method. *J Spinal Disord Tech.* 17:134–139.
- Dakwar E, Cardona RF, Smith DA, Uribe JS. 2010. Early outcomes and safety of the minimally invasive, lateral retroperitoneal transposas approach for adult degenerative scoliosis. *Neurosurgicalfocus.* 28:E8.
- Dreischarf M, Zander T, Shirazi-Adl A, Puttlitz CM, Adam CJ, Chen CS, Goel VK, Kiapour A, Kim YH, Labus KM, et al. 2014. Comparison of eight published static finite element models of the intact lumbar spine: predictive power of models improves when combined together. *J Biomech.* 47:1757–1766.
- Faizan A, Kiapour A, Kiapour AM, Goel VK. 2014. Biomechanical analysis of various footprints of transforaminal lumbar interbody fusion devices. *J Spinal Disord Tech.* 27:E118–E127.
- Grauer JN, Biyani A, Faizan A, Kiapour A, Sairyo K, Ivanov A, Ebraheim NA, Patel TC, Goel VK. 2006. Biomechanics of two-level Charité artificial disc placement in comparison to fusion plus single-level disc placement combination. *Spine J.* 6:659–666.
- Kim KT, Lee SH, Suk KS, Lee JH, Jeong BO. 2010. Biomechanical changes of the lumbar segment after total disc replacement: Charité®, Prodisc® and Maverick® using finite element model study. *J Korean Neurosurg Soc.* 47:446–453.
- Kim HJ, Kang KT, Chang BS, Lee CK, Kim JW, Yeom JS. 2014. Biomechanical analysis of fusion segment rigidity upon stress at both the fusion and adjacent segments: a comparison between unilateral and bilateral pedicle screw fixation. *Yonsei Med J.* 55:1386–1394.
- Kim SJ, Lee YS, Kim YB, Park SW, Hung VT. 2014. Clinical and radiological outcomes of a new cage for direct lateral lumbar interbody fusion. *Korean J Spine.* 11:145–151.
- Knight RQ, Schwaegler P, Hanscom D, Jeffery RQ. 2009. Direct lateral lumbar interbody fusion for degenerative conditions: early complication profile. *J Spinal Disord Tech.* 22:34–37.
- Rohlmann A, Neller S, Claes L, Bergmann G, Wilke HJ. 2001. Influence of a follower load on intradiscal pressure and intersegmental rotation of the lumbar spine. *J Spine.* 26:E557–E561.
- Schmidt H, Heuer F, Drumm J, Klezl Z, Claes L, Wilke HJ. 2007. Application of a calibration method provides more realistic results for a finite element model of a lumbar spinal segment. *Clin Biomech.* 22:377–384.
- Schmidt H, Galbusera F, Rohlmann A, Zander T, Wilke HJ. 2012. Effect of multilevel lumbar disc arthroplasty on spine



- kinematics and facet joint loads in flexion and extension: a finite element analysis. *Eur Spine J.* 21:663–674.
- Sembrano JN, Horazdovsky RD, Sharma AK, Yson SC, Santos EG, Polly DW. 2017. Do lordotic cages provide better segmental lordosis vs. non-lordotic cages in lateral lumbar interbody fusion (LLIF)? *Clin Spine Surg.* 30:E338–E343.
- Shirazi-Adl A, Ahmed AM, Shrivastava SC. 1986. Mechanical response of a lumbar motion segment in axial torque alone and combined with compression. *Spine.* 11:914–927.
- Slucky AV, Brodke DS, Bachus KN, Droge JA, Braun JT. 2006. Less invasive posterior fixation method following transforaminal lumbar interbody fusion: a biomechanical analysis. *Spine J.* 6:78–85.
- Uribe JS, Smith DA, Dakwar E, Baaj AA, Mundis GM, Turner AWL, Cornwall GB, Akbarnia BA. 2012. Lordosis restoration after anterior longitudinal ligament release and placement of lateral hyperlordotic interbody cages in the minimally invasive lateral transpoas approach: a radiographic study in cadavers. *J Neurosurg Spine.* 17:476–485.
- Uribe JS, Harris JE, Beckman JM, Turner AWL, Mundis GM, Akbarnia BA. 2015. Finite element analysis of lordosis restoration with anterior longitudinal ligament release and lateral hyperlordotic cage placement. *Eur Spine J.* 24:420–426.
- Vadapalli S, Sairyo K, Goel VK, Robon M, Biyani A, Khandha A, Ebraheim NA. 2006. Biomechanical rationale for using polyetheretherketone (PEEK) spacers for lumbar interbody fusion—a finite element study. *Spine.* 31:992–998.
- Xiao ZT, Wang LY, Gong H, Zhu D. 2012. Biomechanical evaluation of three surgical scenarios of posterior lumbar interbody fusion by finite element analysis. *Biomed Eng Online.* 11:31.
- Zhang ZJ, Sun YT, Li Y, Liu ZH, Liu WQ. 2016. Recent advances in finite element applications in artificial lumbar disc replacement. *J Biomed Sci Eng.* 9:1–8.
- Zhang ZJ, Li H, Fogel GR, Liao ZH, Li Y, Liu WQ. 2017. Biomechanical analysis of porous additive manufactured cages for lateral lumbar interbody fusion: a finite element analysis. *World Neurosurg.* <https://doi.org/10.1016/j.wneu.2017.12.127> [Epub ahead of print].
- Zhong ZC, Wei SH, Wang JP, Feng CK, Chen CS, Yu CH. 2006. Finite element analysis of the lumbar spine with a new cage using a topology optimization method. *Med Eng Phys.* 28:90–98.